Solution Evaporation-Driven Crumpling and Assembling of Large-Accessible Space,

High-Mechanical Strength Graphene/Carbon Nanotubes Composite Nanoparticles

Qingchang Liu and Baoxing Xu\*

Department of Mechanical and Aerospace Engineering, University of Virginia,

Charlottesville, VA 22904, USA

**ABSTRACT** 

Crumpled graphene particles that are converted and assembled from 2D planar graphene sheets

create a subtle material platform for widespread applications of graphene in a low-cost and

scalable manner. However, such crumpled particles are suffered from small spatial

availabilities in geometry and low strength in mechanical deformation due to the limited

numbers and stabilities of connections among individual deformed graphene. Herein, we report,

in both theoretical analysis and large-scale atomistic simulations, that a crumpled graphene

composite nanoparticle with large accessible space and high-mechanical strength can be

achieved by encapsulating folded carbon nanotubes (CNTs) inside via a solvent evaporation-

induced assembly approach. A unified energy-based theoretical model is developed to address

the kinetic migration of both CNTs and graphene suspended in a liquid droplet and their

crumpling and assembling mechanism into a composite particle by solution evaporation. The

contact probability, surface ridge densities, and geometric size in assembled graphene/CNTs

composite nanoparticles are quantitatively extracted after the complete evaporation of liquid,

and are further correlated with their accessible space including accessible surface area and

volume and mechanical strength. The coarse-grained molecular dynamics simulations are

conducted to uncover structural and morphological evolution of graphene/CNTs composite

nanoparticles with solution evaporation, and the results show remarkable agreement with

theoretical predictions. This study offers a foundation for synthesizing highly connected,

mechanically enhanced, crumpled particles with tunable spatial porous structures by tailoring

graphene and CNTs for applications in functional structures and devices.

KEYWORDS: Crumpling, assembling, composite nanoparticles, spatial connection,

mechanical strength

. .

\* Corresponding author: bx4c@virginia.edu

1/21

## INTRODUCTION

Crumpling multiple pieces of two-dimensional (2D) planar materials such as graphene or graphene oxide into three-dimensional (3D) architectures provides a new powerful strategy for obtaining their bulk form meanwhile remaining the large specific surface area and versatile surface functions of these nanosheets, and has drawn tremendous attention for their widespread applications in the rational design of high-sensitive electronic devices <sup>1-2</sup>, high-power density electrodes <sup>3-6</sup>, electrodes absorbents<sup>7-8</sup>, and high-efficiency gas/liquid filters <sup>9</sup>. To satisfy the desirable requirements in specific applications, the surface of 2D materials could be chemically decorated with functional groups before crumpling and assembling, for example, functionalized graphene with metal oxides SnO2, Fe2O3, or Co3O4 are crumpled into composites for use in lithium-ion batteries with enhanced electron transport<sup>10</sup>. Alternatively, the aerosol-like processing technique has been developed to convert mechanical mixture of nano-sized particles and graphene solution into crumpled graphene composite architectures through rapid evaporation <sup>11-12</sup>. For example, crumpled graphene/Si composites have been synthesized and used in lithium-ion battery with excellent mechanical stability, where the crumpled graphene provides deformation flexibility for accommodating the volume change of Si nanoparticles during charge-discharge cycles<sup>13-14</sup>. Recently, this aerosol-like processing technique has also been utilized to crumple graphene and one-dimensional (1D) nanomaterials mixture into architected composite particles with 3D interconnected structures<sup>5</sup>. Compared with individual isolated nanoparticle components, the 1D nanomaterials could bridge individual crumpled graphene sheets and provide continuous pathways for long-range electron and thermal conduction across crumpled graphene/nanotube composites<sup>15</sup>, offering great potential applications in broad areas such as water purification<sup>16</sup>, supercapacitors <sup>17-18</sup>, conductive yarn<sup>19</sup>, and strain sensors<sup>20-21</sup>. Besides, the 2D geometric nature of graphene could be used to wrap the 1D nanomaterials intensely, thereby promoting the mechanical strength of crumpled particles <sup>5, 7, 22-23</sup>.

Unlike to rigid nanoparticles that usually do not experience any mechanical deformation during solution evaporation, the 1D nanomaterials such as nanotubes and nanowires will be easily deformed, folded, and packed by either crumpling deformation of graphene or dynamic

liquid compression due to their geometric feature of ultra-large aspect ratio<sup>24</sup>. Besides, dispersion behaviors of 2D and 1D materials in liquid solutions could be dramatically different. For example, graphene could migrate to the liquid/air interface in solutions<sup>23, 25-26</sup>, while the carbon nanotubes stay inside the liquid <sup>27-31</sup>, which is expected to influence the subsequent crumpling and assembling process and the formation of 3D spatial networking structures of crumpled composites after complete evaporation of liquid. However, most current studies either focus on the aerosolization process and properties of graphene/nanotubes composites or confine the scope to their various applications, and the underlying fundamental crumpling mechanism is lacking. Thus, the understanding of crumpling mechanism will be of paramount importance for developing efficient, controllable, and general synthetic methods of crumpled 1D/2D composites for practical applications and will also be critical to correlate 3D networking structures of crumpled composites with their spatial features and overall mechanical properties.

In the present study, guided by theoretical predictions and large-scale molecular dynamics simulations, we report a large-accessible space and high-mechanical strength composite particle comprised of crumpled graphene and folded carbon nanotubes (CNTs) by an evaporation-induced assembly approach. We propose an energy-based kinetic migration mechanism of CNTs and graphene mixed solution in a liquid droplet by considering their electrostatic, van der Waals, and their deformation energies under the confinement of capillary force at both equilibrium and dynamic process of the liquid evaporation. Besides, our theory explains the pH-dependent distribution behavior of CNTs and/or graphene. The theoretical analysis shows that the graphene will prefer to accumulate at the liquid/air interface while the CNTs will stay inside the liquid droplet during evaporation. We further propose an encapsulation mechanism of the crumpled graphene/CNTs composite particles and also successfully predict the morphologies of the crumpled particles, including accessible area, pore structure, and surface ridge density. Importantly, we develop an intrinsic material parameter capable of describing the encapsulation state of the composite particles regardless of the types of graphene and CNTs. Moreover, we develop a virtual spherical van der Waal force field that allows to mimic dynamic interactions of liquid with both graphene and CNTs without presence of physical liquid molecules, and establish a coarse-grained molecular dynamics model to

simulate the crumpling and assembling of CNTs and graphene by liquid evaporation in a large-scale and time-efficient fashion. With this computational method, we successfully reproduce the formation of the CNTs-encapsulated crumpled graphene assembled nanoparticles, and fully elucidate the underlying mechanism of crumpling and assembling graphene and CNTs by monitoring the structural evolution of their assembled nanoparticles with liquid solution evaporation. The encapsulation state of graphene over CNTs, accessible spatial area and volume, 3D interconnected network, crumpled surface ridge density, and overall size of assembled particles are extracted and show good agreement with theoretical predictions. In addition, the simulations of uniaxial compression experiments on individual particles show that the mechanical strength depends on crumpled surface ridge density of assembled particles and can be quantitatively predicted in theory.

#### RESULTS AND DISCUSSION

Kinetic Migration Mechanism of CNTs and Graphene in a Liquid Droplet. Figure 1a illustrates a suspension of mixed graphene and CNTs inside a liquid droplet with radius  $R_d$ . Assume the graphene and CNTs are dispersed uniformly in the region  $[r,R_d]$ , where r is the local radial coordinate originating from the geometric center of the droplet, and [0, r] represents the pure liquid region, the total energy of the system at equilibrium is  $E_t = E_{ele} + E_{vdW} + E_{vdW}$  $E_{def} + E_{surf}$ .  $E_{ele}$  is the electrostatic energy of the system and can be estimated by the Derjaguin-Landau-Verwey-Overbeek (DLVO) theory  $^{32-33}$ ,  $E_{vdW}$ ,  $E_{def}$ , and  $E_{surf}$  are van der Waals energy, mechanical deformation energy, and surface energy of graphene and CNTs, respectively <sup>24, 34</sup>, and they all can be theoretically determined (See Supporting Information S1.1). For example, take  $R_d=150$  nm, the total mass concentration of graphene and CNTs in the liquid droplet,  $C_t = 4 \text{ mg/mL}$ , the mass fraction of graphene over the total mass,  $m_g/m_t$ =50%, and aqueous solution pH=7, **Figure 1b** shows the normalized total system energy  $(E_t^r - E_t^{r=0})/E_t^{r=0}$  versus  $r/R_d$ , where  $E_t^{r=0}$  represents the energy of system uniformly distributed by graphene or/and CNTs in the entire liquid droplet. Especially, when only CNTs are suspended in the droplet,  $(E_t^r - E_t^{r=0})/E_t^{r=0}$  shows a monotonous increase with  $r/R_d$ , indicating an energy barrier that prevents CNTs from diffusing toward the outmost surface of droplet. Besides, the larger radius (i.e. chiral number) of CNTs is, the higher the energy barrier

will be because of an increased bending stiffness. As a result, the CNTs are expected to stay inside the droplet at equilibrium. By contrast, when graphene sheets are suspended in the droplet,  $(E_t^r - E_t^{r=0})/E_t^{r=0}$  increases with the increase of  $r/R_d$  for graphene sheets with small areas (e.g.  $n_g$ =80), similar to that of CNTs. For large area graphene (e.g.  $n_g$ =5),  $(E_t^r$  –  $E_t^{r=0}$ )/ $E_t^{r=0}$  shows a decrease with the increase of  $r/R_d$ , indicating that large graphene sheets prefer to stay on the surface of droplet while small ones will stay inside the liquid droplet, which agrees well with experimental observations <sup>25-26</sup>. In addition, the pH of liquid solution will change the surface charge density of graphene and CNTs <sup>33, 35-36</sup> (See Figure S1) and influence the electrostatic as well as the total energy of the system (Figure 1c)<sup>33, 35-36</sup>. Consequently, the distribution of graphene and CNTs will vary with the pH of liquid solutions. For example, at pH=12, there is a large energy barrier preventing graphene sheets from migrating to the droplet surface. When pH decreases to as low as 4, the energy barrier diminishes, which energetically leads to the migration of graphene sheets to the outmost surface of droplet. This pH-dependent behavior provides an option to tune the position of graphene in the dispersion, similar to observations in experiments<sup>26</sup>. For CNTs, regardless of size, there is always preferable in energy to support their stay inside of droplet. In practice, the size of graphene sheets in experiments is always beyond hundreds of nanometers<sup>37</sup>, therefore, the graphene sheets usually stay at the surface of droplet while CNTs stay inside the droplet with a uniform distribution, as observed in experiments<sup>38</sup>. Therefore, when all the graphene sheets have migrated to the surface of droplet either at equilibrium or during the liquid evaporation, the total area of graphene can be calculated via  $A_g^t = \omega C_t V_d/
ho_g$  , where  $\omega = m_g/m_t, V_d = 4\pi R_d^3/3$ ,  $\rho_g$  is the mass density of graphene per area, and the surface area of the droplet is  $A_d = 4\pi R_d^2$ . When  $A_g^t > A_d$ , the droplet is completely wrapped by graphene, referred to here as "complete wrapping status". When  $A_g^t < A_d$ , the droplet is partially wrapped by graphene, referred to here as "partial wrapping status".  $A_g^t = A_d$  corresponds to the critical transition status of the droplet from "complete-wrapping" to "partial-wrapping", which leads to  $\omega = 3\rho_g/C_tR_d$ . Figure 1d plots the variation of this critical transition with  $m_g/m_t$  and  $C_t$  for different droplet sizes. A low  $C_t$  will benefit the initial formation of "partial-wrapping  $(A_g^t < A_d)$ " status, and a large droplet size will promote the transition from

"partial-wrapping  $(A_g^t > A_d)$ " to "complete-wrapping  $(A_g^t > A_d)$ " status. This transition will also hold during the liquid evaporation. For example, when the liquid evaporation occurs,  $m_g/m_t$  will remain constant while  $R_d$  will decrease, and thus the total mass concentration  $C_t$  will increase, leading to in a transition of the liquid surface from "partial-wrapping  $(A_g^t > A_d)$ " to "complete-wrapping  $(A_g^t > A_d)$ " status.

Encapsulation Mechanism of the Crumpled Graphene/CNTs Composite Particles. With the migration behavior of CNTs and graphene at both equilibrium and liquid evaporation stages, Figure 2a shows the schematic illustration of crumpling and assembling graphene and CNTs by liquid evaporation. Assume the droplet is sufficiently large enough, with the liquid evaporation, graphene sheets will migrate and accumulate to the surface of droplet, and CNTs stay inside. The continuous evaporation will crumple the graphene on the droplet surface and pack the CNTs inside the droplet, and a CNTs-encapsulated, crumpled graphene composite nanoparticle will be eventually formed after the complete evaporation of liquid, similar to the observations in experiments on the formation of a thin outer layer of graphene coating on the folded CNTs<sup>5</sup>. Further analysis shows that the overall size and morphologies of the composite nanoparticles rely on the competition between the packing of CNTs inside and the crumpling of graphene on the surface (See Supporting Information S1.2-1.3 and Figures S2 and S3) and can also be tuned by the mass fraction of graphene (i.e.  $m_q/m_t$ ) and radius of CNTs. Assume the radius of crumpled particles by pure graphene and CNTs is  $R_p^g$  and  $R_p^c$ , respectively, the radius of their composite particles can be defined by  $R_p^h =$  $\left(R_p^c\right)^{1-m_g/m_t}\left(R_p^g\right)^{m_g/m_t}$ . If  $R_p^g < R_p^h$ , the CNTs cannot be completely wrapped by graphene, and the composite particles will have an "open-cell" structure. If  $R_p^g \ge R_p^h$ , CNTs will be fully encapsulated by graphene, and the composite particles will have a "closed core-shell" structure. Take  $R_d=150$  nm and  $C_t=4$  mg/mL as an example, **Figure 2b** plots the variation of  $R_p^g$ ,  $R_p^c$ and  $R_p^h$  with  $m_g/m_t$ . At  $R_p^g = R_p^c = R_p^h$ , the critical  $m_g/m_t$  that leads to an "open-celled" or "closed core-shell" structure of composite particles can be obtained, and it increases with the increase of CNTs radius. To further reflect the competition between the packing of CNTs and

crumpling of graphene, an intrinsic parameter,  $B_g A_g^t/B_c L_c^t$  (**Figure 2c**), is proposed to describe the transition of particles morphologies from "open-celled" to "closed core-shell" status, where  $B_g$  and  $A_g^t$  are the bending stiffness and total area of graphene, respectively, and  $B_c$  and  $L_c^t$  are the bending stiffness and total length of CNTs, respectively. The analysis shows the critical  $B_g A_g^t/B_c L_c^t = 0.012$  for the transition, regardless of the types of CNTs or  $m_g/m_t$ , which agrees well with our simulation results (See **Supporting Information S2.1-2.2** and **Figures S4-S6**). This transition is also observed in experiments, for example, with the approximate estimations to available experimental results<sup>5</sup> (See **Supporting Information**, **Table S1**),  $B_g A_g^t/B_c L_c^t$  is 0.01094 and 0.05472 for "open-celled" and "closed core-shell" particles, respectively, which shows a reasonable agreement with our theoretical prediction of the encapsulating transition value  $B_g A_g^t/B_c L_c^t = 0.012$ .

Interconnected 3D Networking Structures and Spatial Properties of Crumpled Graphene/CNTs Composite Particles. Figure 3a shows the morphology of the crumpled composite particles from simulations at different  $m_g/m_t$  and diameters of CNTs. The CNTs and the graphene are highlighted in red and blue, respectively, and the graphene in blue is further rendered in 50% transparency to facilitate the observations of crumpled and interconnected spatial 3D structures. To characterize the surface morphology of each crumpled particle, the radius  $R_p^h$  in the simulations is calculated (See Supporting Information S2.3 and Figure S7) and their corresponding equivalent sphere is constructed (Figure S8). This equivalent sphere also allows extracting the surface pore ratio  $(P_r)$  of the crumpled particle.  $P_r$ is defined by dividing the surface area not covered by graphene sheets (pore) over the total surface area of the crumpled particle (See Supporting Information S2.3 and Figure S9). At the same time,  $P_r$  can be calculated based on the radii of particles predicted by our theory and is  $P_r = 1 - A_p^g / A_p^h$ , where  $A_p^g = 4\pi (R_p^g)^2$  and  $A_p^h = 4\pi (R_p^h)^2$  are the surface area of particles assembled by pure graphene and hybrid CNTs and graphene, respectively. That is, we will have  $P_r=1-(R_p^g/R_p^h)^2$ , and  $R_p^g/R_p^h$  reflects the crumpling intensity.  $P_r$  decreases with the increase of  $m_g/m_t$  and small CNTs lead to small  $P_r$  (Figure S10). Figure 3b plots  $P_r$  versus  $(R_p^g/R_p^h)^2$ . Good agreement is obtained between the theoretical predictions and simulations. Especially, at  $R_p^g/R_p^h$ =0, there is no graphene, and  $P_r$ =100 %; at  $R_p^g/R_p^h \ge 1$ , the CNTs are fully encapsulated by graphene, and  $P_r$ =0; and at  $0 < R_p^g/R_p^h < 1$ , the particle surface will be partially wrapped by graphene. Further, we define a critical pore ratio  $P_r^c = 5\%$  in the simulations to describe the transition from "open-celled" to "closed core-shell" structure of composite particles, and the corresponding critical  $m_g/m_t$  can be obtained and is plotted in **Figure 3a**, which agrees well with theoretical predictions. Besides, the theoretical analysis shows  $P_r \propto -\left[\left(R_p^g\right)^{1-m_g/m_t}/\left(R_p^c\right)^{1-m_g/m_t}\right]^2$  and  $R_p^c \propto B_c L_c^t$ ,  $R_p^g \propto B_g A_g^t$  (See **Supporting Information S1.4**), and therefore the characterization of wrapping status can be unified by  $B_g A_g^t/B_c L_c^t$ . **Figure 3c** plots  $P_r$  versus  $B_g A_g^t/B_c L_c^t$ , and a linear relationship is obtained, independent of CNT sizes, which also agrees well with the theoretical predictions.

Figure 3d shows the variation of the specific accessible surface area  $A_{cs}$  in crumpled particles normalized by  $A_{surf}$  with  $m_g/m_t$ , where  $A_{surf}=A_c(1-m_g/m_t)+A_gm_g/m_t$ ,  $A_c$  is the intrinsic surface area of CNT (e.g.  $A_c$ =1315  $m^2/g$  for single-walled CNT) and  $A_g$  is the intrinsic surface area of graphene (e.g.  $A_g=2630 \ m^2/g$  for single-layer graphene)<sup>39</sup>. We should note that both the surface area of graphene/CNT inside and on the surface of the particles can be accessed in "open-cell" crumpled particles, but only the surface area is accessible in "closed core-shell" crumpled particles (See Supporting Information S2.3 and Figures S11-S14). At a low  $m_g/m_t$ , the crumpled particle is open and shows a high  $A_{cs}/A_{surf}$ . With the increase of  $m_g/m_t$ , the crumpled particle becomes a closed core-shell structure and shows a rapid decrease of  $A_{cs}/A_{surf}$ . Besides,  $A_{cs}/A_{surf}$  shows a strong dependence on the size of CNTs due to the close relevance to wrapping status by graphene. In theory, we also calculate the accessible surface areas (See Supporting Information S1.5) and plot them in Figure 3d, and good agreement between theoretical predictions and simulations are obtained. The further comparison of the normalized accessible surface area of the particles between our theoretical prediction and available experimental data<sup>5</sup> validates our theory (See Supporting Information, Table S2).

Figure 3e illustrates the variation of the spatial "pore" volume  $V_{pore}$  over the particle volume  $V_{particle}$ ,  $V_{pore}/V_{particle}$ , with  $m_g/m_t$ . The pore volume is obtained by examining the spatial distribution of pore sizes across an entire assembled particle  $^{40\text{-}41}$  (See Figures S15-S17), and the volume of the overall particle is calculated via  $V_{particle}=4\pi\left(R_p^h\right)^3/3$ . Similar to that of accessible area, only the pores that are accessible to the external molecules/atoms are taken into account in the calculation of spatial pore volume. At a low  $m_g/m_t$ , the crumpled particle is open and shows a high  $V_{pore}/V_{particle}$ . With the increase of  $m_g/m_t$ , the crumpled particle becomes a closed core-shell structure, and  $V_{pore}/V_{particle}$  shows a rapid decrease. In addition,  $V_{pore}/V_{particle}$  shows a strong dependence on the size of CNTs due to the close relevance to wrapping status of assembled particles by graphene. Similar to Figure 3d, the normalized pore volume is also extracted in theory (See Supporting Information S1.6) and shows good agreement with simulations (Figure 3e).

Surface Morphology, Ridge density, and Mechanical Stiffness of Crumpled Graphene/CNTs Composite Particles. Figure 4a shows the surface morphology of the crumpled particles with highlights on the local deformation curvature, where the local curvature can be calculated from the deformation energy (See Supporting Information S2.3). Further, if the local curvature due to bending deformation is larger than 0.5  $nm^{-1}$ , we will define such the sharp local deformation as a ridge<sup>42</sup>. The equivalent sphere is also given to reflect the distribution of ridges on the surface of crumpled particles (Figure S18), and where the total length of ridges in graphene over the entire surface area of the crumpled particle is defined as the ridge density ( $D_T$ , in nm<sup>-1</sup>), and is calculated using the image processing technique (Figure S19)<sup>42</sup>. For the crumpling with a (5,5) CNT at  $m_g/m_t$ =25%, the ridges only exist in the localized area due to partial encapsulation of CNTs by crumpled graphene. When  $m_g/m_t$  increases to 75%, the crumpling of graphene becomes sever with CNTs fully encapsulated inside, and more ridges appear. Similar results are also observed for the crumpled particles with large (10,10) and (15,15) CNTs. The equivalent radius of particles and ridge density ( $R_p^h, D_T$ ) are also denoted in Figure 4a. In theory, the ridge density can be obtained

from the analysis on deformation energy of graphene in the hybrid particles and is characterized as a function of  $R_p^g/R_p^h$  (See **Supporting Information S1.7**), similar to Figure 3b. **Figure 4b** shows the comparison of  $D_r$  between the theoretical predictions and simulation results with good agreement. More importantly, at  $R_p^g/R_p^h=0$ , there is no graphene in the particle, and  $D_r=0$ ; at  $R_p^g/R_p^h>1$ , a large  $D_r$  is obtained, indicating the packed CNTs inside enhance crumpling of graphene. **Figure 4c** further plots the variation of  $D_r$  with the unified material parameter  $B_g A_g^t/B_c L_c^t$ , and a good linear relationship is obtained, similar to Figure 3c.

The introduction of surface morphologies to graphene or CNTs usually will lead to a change of its mechanical properties<sup>43</sup>. Especially, high roughness such as local ridges are expected to enhance deformation resistance of structures to mechanical loadings 44-45. To investigate the mechanical performance of the crumpled particles, the compression test on a single composite particle is conducted (See Supporting Information S2.4 for simulation model and method and simulation snapshots in Figures S20). Figure 5a plots the force (F)displacement (h) curves of graphene/(10,10) CNTs hybrid particle. The Young's modulus  $E_{eff}$ can be obtained with Hertz contact theory via  $F = \frac{4E_{eff}(R_p^h)^{1/2}}{3(1-v^2)} \left(\frac{h}{2}\right)^{\frac{3}{2}}$ , where v is the Poisson's ratio and is taken 0.3  $^{46}$ . Note that the  $E_{eff}$  is averaged by performing compression experiments in three directions (Figures S21-S24), and it shows a clear dependence of both  $m_g/m_t$  and CNTs size. To further understand the effect of surface ridge density on  $E_{eff}$ , Figure 5b shows the variation of  $E_{eff}$  with  $D_r$ .  $E_{eff}$  increases linearly with  $D_r$ , suggesting that the local curvature could be utilized to enhance the mechanical properties of crumpled graphene particles and can be adjusted by mixing CNTs in liquid solution. The variation of  $E_{eff}$  with the unified material parameter  $B_g A_g^t / B_c L_c^t$  is also illustrated, and it also shows a very good linear relationship, similar to Figure 3c.

# **CONCLUSIONS**

In summary, we demonstrate that the graphene and CNTs mixture suspended in a liquid droplet can be crumpled and assembled into a composite nanoparticle by solution evaporation, and the

assembled composite nanoparticles exhibit a large-accessible spatial performance and highmechanical strength in comparison with that of either crumpling graphene or CNTs only. We have developed a unified energy-based migration model and show that the graphene will prefer to migrate and accumulate at the liquid/air interface while the CNTs stay inside the liquid droplet. This migration model also confirms the formation of CNTs-encapsulated, crumpled graphene assembled composite nanoparticles by solution evaporation. Further, guided by the molecular dynamics simulations, we have systemically investigated the crumpling and assembling of graphene and CNTs by the liquid evaporation and monitored the evolution of crumpled graphene/CNTs composite particles. The effect of CNTs size and mass fraction of graphene on the crumpled composite particles, including surface crumpling morphology, overall size, and the accessible surface area and spatial volume, is elucidated. In particular, the spatial 3D interconnected contacts between CNTs and graphene are extracted and are also theoretically correlated with the geometric and mechanical properties of CNTs and graphene with remarkable agreement. Besides, the crumpled surface roughness, referred to as ridge density, is quantitatively characterized and its linear relationship with the mechanical strength of assembled particles is established by conducting uniaxial compression tests. The assembled composite nanoparticles will help seek structurally spatial wrapping, high accessible surface area, versatile surface morphologies, and mechanically strong nanoparticles, for potential applications in functional structures and devices in the fields of thermal transport<sup>47</sup>, electronics<sup>5</sup>, energy absorption<sup>11, 48</sup>, water treatment<sup>49</sup> and solar cells<sup>50</sup>, and could also serve as the unit building blocks for assembling large-scale quantities of graphene, CNTs and their hybrids. The fundamental mechanisms elucidated will provide immediate guidance to tune the formation of crumpled graphene/CNTs composite particles from the overall size to ridge density and could also be extended to study of crumpling and assembling other materials encapsulated composite nanoparticles in a broad of low-dimensional nanomaterials such as nanowires, nanoparticles, and nanofibers through the aerosol-like processing technique.

# ASSOCIATED CONTENT

# SUPPORTING INFORMATION

Migration model of graphene and CNT in droplet. The theoretical models of packing CNTs and

crumpling graphene by the liquid evaporation. Size of the graphene/CNTs composite particles. Surface pore ratio of the graphene/CNTs composite particles. The accessible surface area of the graphene/CNTs composite particles. Pore volume of the graphene/CNTs composite particles. Surface ridge density of the graphene/CNTs composite particles. Coarse-grained molecular dynamics modeling. Virtual spherical van der Waals simulation method. Characterization of the particles. Simulations of Uniaxial Compression on Particles

## **AUTHOR INFORMATION**

#### **CORRESPONDING AUTHOR**

**Baoxing Xu-** Department of Mechanical and Aerospace Engineering, University of Virginia, Charlottesville, VA 22904, USA. Email: <u>bx4c@virginia.edu</u>.

## **AUTHORS**

**Qingchang Liu-** Department of Mechanical and Aerospace Engineering, University of Virginia, Charlottesville, VA 22904, USA

**Baoxing Xu-** Department of Mechanical and Aerospace Engineering, University of Virginia, Charlottesville, VA 22904, USA

# **NOTES**

The authors declare no competing financial interest.

## **ACKNOWLEDMENTS**

This work is supported by NSF-CMMI-1928788 and the start-up funds at the University of Virginia.

## **REFERENCES**

- (1) Lou, Z.; Chen, S.; Wang, L.; Jiang, K.; Shen, G. An ultra-sensitive and rapid response speed graphene pressure sensors for electronic skin and health monitoring. *Nano Energy* **2016**, *23*, 7-14.
- (2) Paul, R. K.; Badhulika, S.; Saucedo, N. M.; Mulchandani, A. Graphene nanomesh as highly sensitive chemiresistor gas sensor. *Analytical chemistry* **2012**, *84* (19), 8171-8178.

- (3) Chen, K.; Song, S.; Liu, F.; Xue, D. Structural design of graphene for use in electrochemical energy storage devices. *Chemical Society Reviews* **2015**, *44* (17), 6230-6257.
- (4) Stoller, M. D.; Park, S.; Zhu, Y.; An, J.; Ruoff, R. S. Graphene-based ultracapacitors. *Nano letters* **2008**, *8* (10), 3498-3502.
- (5) Yang, J.; Sun, H.; Liang, H.; Ji, H.; Song, L.; Gao, C.; Xu, H. A highly efficient metal-free oxygen reduction electrocatalyst assembled from carbon nanotubes and graphene. *Advanced materials* **2016**, *28* (23), 4606-13, DOI: 10.1002/adma.201505855.
- (6) Wang, G.; Xing, W.; Zhuo, S. The production of polyaniline/graphene hybrids for use as a counter electrode in dye-sensitized solar cells. *Electrochimica Acta* **2012**, *66*, 151-157.
- (7) Sohn, K.; Joo Na, Y.; Chang, H.; Roh, K. M.; Dong Jang, H.; Huang, J. Oil absorbing graphene capsules by capillary molding. *Chemical communications* **2012**, *48* (48), 5968-70, DOI: 10.1039/c2cc32049e.
- (8) Liu, Y.; Ma, J.; Wu, T.; Wang, X.; Huang, G.; Liu, Y.; Qiu, H.; Li, Y.; Wang, W.; Gao, J. Cost-effective reduced graphene oxide-coated polyurethane sponge as a highly efficient and reusable oil-absorbent. *ACS applied materials & interfaces* **2013**, *5* (20), 10018-10026.
- (9) Liu, Y.; Lee, J. H. D.; Xia, Q.; Ma, Y.; Yu, Y.; Yung, L. Y. L.; Xie, J.; Ong, C. N.; Vecitis, C. D.; Zhou, Z. A graphene-based electrochemical filter for water purification. *Journal of Materials Chemistry A* **2014**, *2* (39), 16554-16562.
- (10) Li, X.; Qi, W.; Mei, D.; Sushko, M. L.; Aksay, I.; Liu, J. Functionalized graphene sheets as molecular templates for controlled nucleation and self-assembly of metal oxide-graphene nanocomposites. *Advanced materials* **2012**, *24* (37), 5136-5141.
- (11) Luo, J.; Jang, H. D.; Sun, T.; Xiao, L.; He, Z.; Katsoulidis, A. P.; Kanatzidis, M. G.; Gibson, J. M.; Huang, J. Compression and aggregation-resistant particles of crumpled soft sheets. *ACS nano* **2011**, *5* (11), 8943-8949.
- (12) Xu, B.; Rogers, J. A. Mechanics-driven approaches to manufacturing—A perspective. *Extreme Mechanics Letters* **2016**, *7*, 44-48.
- (13) Lee, J. K.; Smith, K. B.; Hayner, C. M.; Kung, H. H. Silicon nanoparticles-graphene paper composites for Li ion battery anodes. *Chemical communications* **2010**, *46* (12), 2025-2027.
- (14) Wang, J.-Z.; Zhong, C.; Chou, S.-L.; Liu, H.-K. Flexible free-standing graphene-silicon composite film for lithium-ion batteries. *Electrochemistry Communications* **2010**, *12* (11), 1467-1470.
- (15) Pham, G. T.; Park, Y. B.; Wang, S.; Liang, Z.; Wang, B.; Zhang, C.; Funchess, P.; Kramer, L. Mechanical and electrical properties of polycarbonate nanotube buckypaper composite sheets. *Nanotechnology* **2008**, *19* (32), 325705, DOI: 10.1088/0957-4484/19/32/325705.
- (16) Sui, Z.; Meng, Q.; Zhang, X.; Ma, R.; Cao, B. Green synthesis of carbon nanotube—graphene hybrid aerogels and their use as versatile agents for water purification. *Journal of Materials Chemistry* **2012**, *22* (18), 8767-8771.
- (17) Cheng, Q.; Tang, J.; Ma, J.; Zhang, H.; Shinya, N.; Qin, L. C. Graphene and carbon nanotube composite electrodes for supercapacitors with ultra-high energy density. *Physical chemistry chemical physics : PCCP* **2011**, *13* (39), 17615-24, DOI: 10.1039/c1cp21910c.
- (18) Jung, N.; Kwon, S.; Lee, D.; Yoon, D. M.; Park, Y. M.; Benayad, A.; Choi, J. Y.; Park, J. S. Synthesis of chemically bonded graphene/carbon nanotube composites and their application in large volumetric capacitance supercapacitors. *Advanced materials* **2013**, *25* (47), 6854-8, DOI: 10.1002/adma.201302788.
- (19) Foroughi, J.; Spinks, G. M.; Antiohos, D.; Mirabedini, A.; Gambhir, S.; Wallace, G. G.; Ghorbani, S. R.; Peleckis, G.; Kozlov, M. E.; Lima, M. D. Highly conductive carbon nanotube-graphene hybrid yarn. *Advanced Functional Materials* **2014**, *24* (37), 5859-5865.
- (20) Liu, H.; Gao, J.; Huang, W.; Dai, K.; Zheng, G.; Liu, C.; Shen, C.; Yan, X.; Guo, J.; Guo, Z. Electrically conductive strain sensing polyurethane nanocomposites with synergistic carbon nanotubes and graphene bifillers.

- Nanoscale 2016, 8 (26), 12977-89, DOI: 10.1039/c6nr02216b.
- (21) Shi, J.; Li, X.; Cheng, H.; Liu, Z.; Zhao, L.; Yang, T.; Dai, Z.; Cheng, Z.; Shi, E.; Yang, L.; Zhang, Z.; Cao, A.; Zhu, H.; Fang, Y. Graphene reinforced carbon nanotube networks for wearable strain sensors. *Advanced Functional Materials* **2016**, *26* (13), 2078-2084, DOI: 10.1002/adfm.201504804.
- (22) Chen, Y.; Guo, F.; Jachak, A.; Kim, S. P.; Datta, D.; Liu, J.; Kulaots, I.; Vaslet, C.; Jang, H. D.; Huang, J.; Kane, A.; Shenoy, V. B.; Hurt, R. H. Aerosol synthesis of cargo-filled graphene nanosacks. *Nano letters* **2012**, *12* (4), 1996-2002, DOI: 10.1021/nl2045952.
- (23) Chen, Y.; Guo, F.; Qiu, Y.; Hu, H.; Kulaots, I.; Walsh, E.; Hurt, R. H. Encapsulation of particle ensembles in graphene nanosacks as a new route to multifunctional materials. *ACS nano* **2013**, *7* (5), 3744-53, DOI: 10.1021/nn3055913.
- (24) Liu, Q.; Xu, B. Liquid-evaporation-assisted self-folding of one-dimensional nanomaterials. *The Journal of Physical Chemistry C* **2018**, *122* (5), 3078-3090.
- (25) Kim, J.; Cote, L. J.; Kim, F.; Huang, J. Visualizing graphene based sheets by fluorescence quenching microscopy. *Journal of the American Chemical Society* **2009**, *132* (1), 260-267.
- (26) Kim, J.; Cote, L. J.; Kim, F.; Yuan, W.; Shull, K. R.; Huang, J. Graphene oxide sheets at interfaces. *Journal of the American Chemical Society* **2010**, *132* (23), 8180-8186.
- (27) Zhao, W.; Song, C.; Pehrsson, P. E. Water-soluble and optically pH-sensitive single-walled carbon nanotubes from surface modification. *Journal of the American Chemical Society* **2002**, *124* (42), 12418-9, DOI: 10.1021/ja027861n.
- (28) Imasaka, K.; Khaled, U.; Wei, S.; Suehiro, J. pH dependence of water-solubility of single-walled carbon nanotubes treated by microplasma in aqueous solution. *Electroanalysis* **2004**, *16*.
- (29) Lin, D.; Liu, N.; Yang, K.; Zhu, L.; Xu, Y.; Xing, B. The effect of ionic strength and pH on the stability of tannic acid-facilitated carbon nanotube suspensions. *Carbon* **2009**, *47* (12), 2875-2882, DOI: 10.1016/j.carbon.2009.06.036.
- (30) Yang, Q.; Li, X.; Zhang, L.; Wang, G.; Chen, G.; Lin, D.; Xing, B. Dispersion and stability of multi-walled carbon nanotubes in water as affected by humic acids. *Journal of Molecular Liquids* **2019**, *279*, 361-369, DOI: 10.1016/j.molliq.2019.01.143.
- (31) Pramanik, C.; Gissinger, J. R.; Kumar, S.; Heinz, H. Carbon nanotube dispersion in solvents and polymer solutions: mechanisms, assembly, and preferences. *ACS nano* **2017**, *11* (12), 12805-12816, DOI: 10.1021/acsnano.7b07684.
- (32) Wu, L.; Gao, B.; Tian, Y.; Munoz-Carpena, R.; Zigler, K. J. DLVO interactions of carbon nanotubes with isotropic planar surfaces. *Langmuir : the ACS journal of surfaces and colloids* **2013**, *29* (12), 3976-88, DOI: 10.1021/la3048328.
- (33) Gudarzi, M. M. Colloidal stability of graphene oxide: aggregation in two dimensions. *Langmuir: the ACS journal of surfaces and colloids* **2016,** *32* (20), 5058-68, DOI: 10.1021/acs.langmuir.6b01012.
- (34) Liu, Q.; Xu, B. Two-and three-dimensional self-folding of free-standing graphene by liquid evaporation. *Soft matter* **2018**, *14* (29), 5968-5976.
- (35) Sun, T.; Zhuo, Q.; Liu, X.; Sun, Z.; Wu, Z.; Fan, H. Hydrophobic silica aerogel reinforced with carbon nanotube for oils removal. *Journal of Porous Materials* **2014**, *21* (6), 967-973, DOI: 10.1007/s10934-014-9845-0
- (36) Kim, J.; Cote, L. J.; Kim, F.; Yuan, W.; Shull, K. R.; Huang, J. Graphene oxide sheets at interfaces. *Journal of the American Chemical Society* **2010**, *132* (23), 8180-6, DOI: 10.1021/ja102777p.
- (37) Zhang, L.; Liang, J.; Huang, Y.; Ma, Y.; Wang, Y.; Chen, Y. Size-controlled synthesis of graphene oxide sheets on a large scale using chemical exfoliation. *Carbon* **2009**, *47* (14), 3365-3368.

- (38) Kim, D. H.; Yun, Y. S.; Jin, H.-J. Difference of dispersion behavior between graphene oxide and oxidized carbon nanotubes in polar organic solvents. *Current Applied Physics* **2012**, *12* (3), 637-642, DOI: 10.1016/j.cap.2011.09.015.
- (39) Peigney, A.; Laurent, C.; Flahaut, E.; Bacsa, R.; Rousset, A. Specific surface area of carbon nanotubes and bundles of carbon nanotubes. *Carbon* **2001**, *39* (4), 507-514.
- (40) Bhattacharya, S.; Gubbins, K. E. Fast method for computing pore size distributions of model materials. *Langmuir: the ACS journal of surfaces and colloids* **2006**, *22* (18), 7726-7731.
- (41) Kappel, F.; Kuntsevich, A. V. An implementation of Shor's r-algorithm. *Computational Optimization and Applications* **2000**, *15* (2), 193-205.
- (42) Liu, Q.; Huang, J.; Xu, B. Evaporation-driven crumpling and assembling of two-dimensional (2D) materials: A rotational spring-mechanical slider model. *Journal of the Mechanics and Physics of Solids* **2019**, *133*, 103722.
- (43) Zhang, T.; Li, X.; Gao, H. Fracture of graphene: a review. *International Journal of Fracture* **2015**, *196* (1-2), 1-31
- (44) Matan, K.; Williams, R. B.; Witten, T. A.; Nagel, S. R. Crumpling a thin sheet. *Physical review letters* **2002**, 88 (7), 076101.
- (45) Deboeuf, S.; Katzav, E.; Boudaoud, A.; Bonn, D.; Adda-Bedia, M. Comparative study of crumpling and folding of thin sheets. *Physical review letters* **2013**, *110* (10), 104301.
- (46) Zhao, P.; Shi, G. Study of Poisson's ratios of graphene and single-walled carbon nanotubes based on an improved molecular structural mechanics model. *Structural Longevity* **2011**, *5* (1), 49-58.
- (47) Zhang, J.; He, X.; Yang, L.; Wu, G.; Sha, J.; Hou, C.; Yin, C.; Pan, A.; Li, Z.; Liu, Y. Effect of tensile strain on thermal conductivity in monolayer graphene nanoribbons: a molecular dynamics study. *Sensors* **2013**, *13* (7), 9388-9395.
- (48) Yang, W.; Yue, Z.; Xu, B. A hybrid elastomeric foam-core/solid-shell spherical structure for enhanced energy absorption performance. *International Journal of Solids and Structures* **2016**, *92*, 17-28.
- (49) Sohn, K.; Na, Y. J.; Chang, H.; Roh, K.-M.; Jang, H. D.; Huang, J. Oil absorbing graphene capsules by capillary molding. *Chemical communications* **2012**, *48* (48), 5968-5970.
- (50) Hao, W.; Chiou, K.; Qiao, Y.; Liu, Y.; Song, C.; Deng, T.; Huang, J. Crumpled graphene ball-based broadband solar absorbers. *Nanoscale* **2018**, *10* (14), 6306-6312.

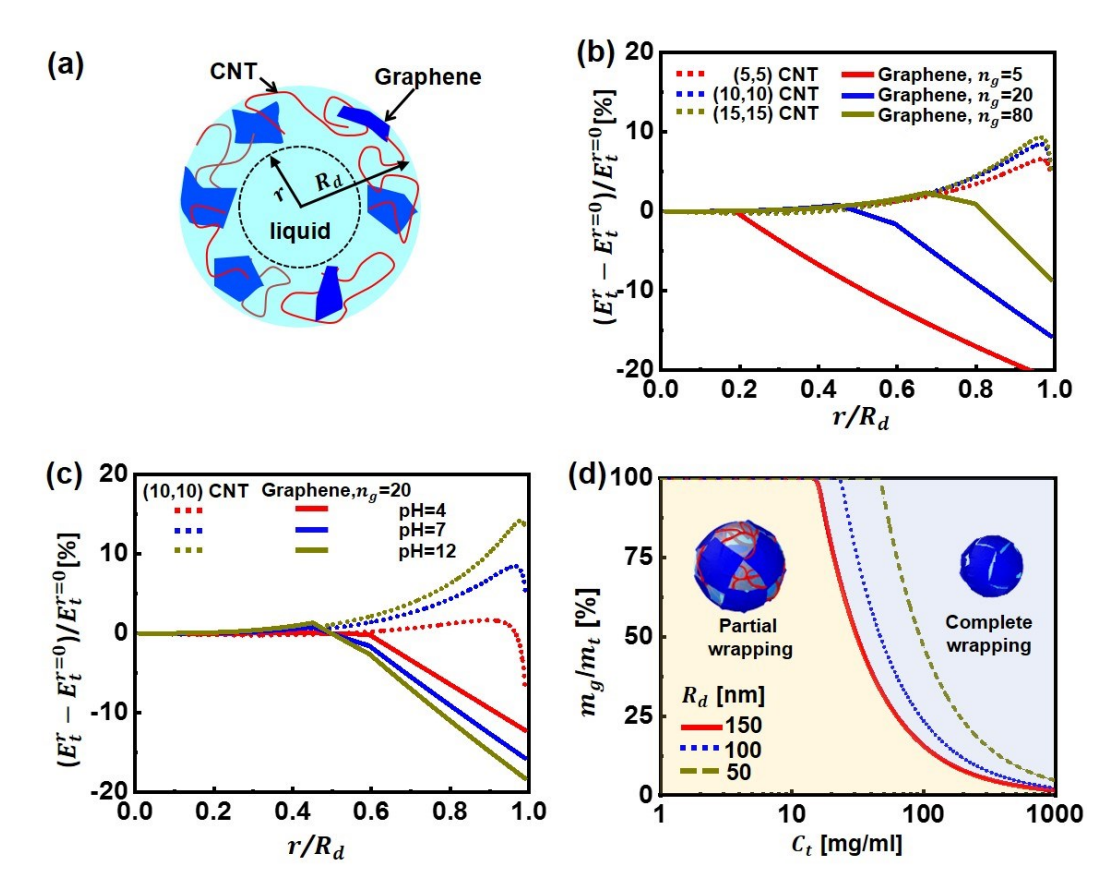


Figure 1. Kinetic migration model of CNTs and graphene in a liquid droplet. (a) Schematics of graphene and CNTs suspended inside a liquid droplet.  $R_d$  is the radius of droplet and r is the local coordinate originating from the center of the droplet. (b) The normalized total system energy  $(E_t^r - E_t^{r=0})/E_t^{r=0}$  for different sizes of CNTs and graphene sheets at pH=7.  $E_t^{r=0}$  represents the energy of system uniformly filled by graphene or CNTs without pure liquid region (r=0). The geometric shape of graphene is square with the total area of  $A_g^t$ =37100  $nm^2$  and  $n_g$  is the number of graphene sheets. The total length and radius of CNTs are 17380 nm and 0.339 nm for (5,5) CNTs, 8700 nm and 0.678nm for (10,10) CNTs, and 5800 nm and 1.017nm for (15,15) CNTs. (c) Effect of pH on the normalized total system energy  $(E_t^r - E_t^{r=0})/E_t^{r=0}$ . (d) Phase diagram of surface status of liquid droplet under the mass fraction of graphene over the total mass of CNTs and graphene  $m_g/m_t$  and concentration of graphene/CNTs mixture  $(C_t)$  at different size of droplet.

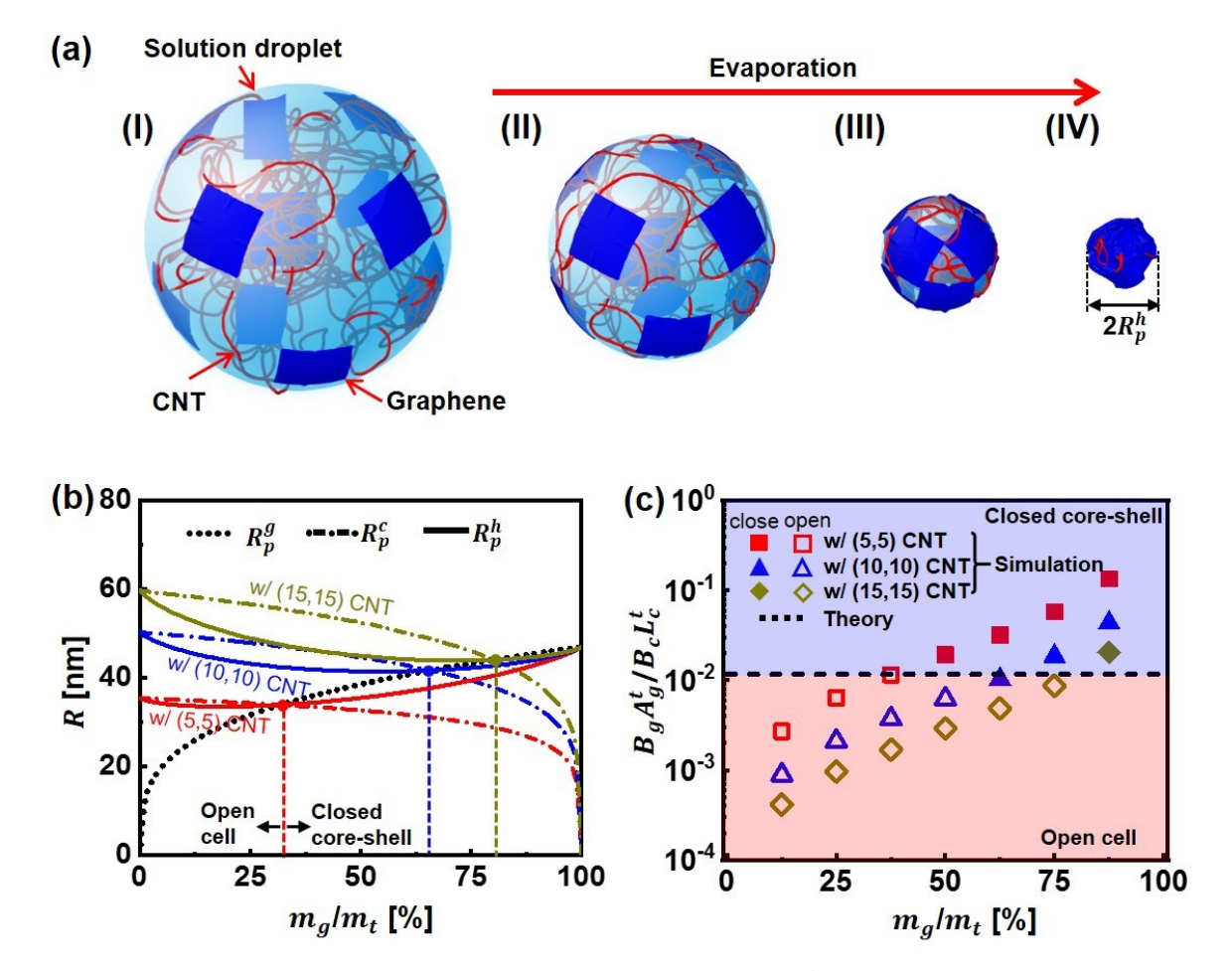


Figure 2. Size and wrapping status of crumpled graphene/CNT composite particles. (a) Schematics of crumpling graphene/CNTs mixture with the evaporation of liquid solution. At the early stage of evaporation (stage I and II), the graphene sheets begin to migrate and accumulate at the liquid/air interface; the CNTs stay inside the droplet and only a small portion pierces the droplet surface and exposes to air. With the continuous evaporation of liquid (stage III), the graphene sheets on the liquid surface will be crumpled and assembled, and the CNTs inside the droplet will be deformed and packed, which eventually lead to the formation of the CNT-encapsulated crumpled graphene assembled nanoparticles after complete evaporation of liquid (stage IV). (b) Theoretical prediction on the size of crumpled hybrid particles  $(R_p^h)$  at

different  $m_g/m_t$ .  $R_p^g$  and  $R_p^c$  show the size of crumpled particle with only graphene and CNTs in an initial droplet liquid, respectively. The radius of the initial droplet  $R_d$  is 150 nm and the concentration of graphene/CNTs in droplet solution  $C_t$  is 4 mg/mL. (c) Comparison of pore structures between theoretical predictions and simulation results.  $B_g$  and  $A_g^t$  are the bending stiffness and total area of graphene, respectively;  $B_c$  and  $L_c^t$  are the bending stiffness and total length of CNTs, respectively. The critical  $B_g A_g^t/B_c L_c^t = 0.012$  can be obtained in theory regardless of CNTs size and  $C_t$ . At  $B_g A_g^t/B_c L_c^t > 0.012$ , the crumpled composite particles are

"closed core-shell" structure and at  $B_g A_g^t/B_c L_c^t < 0.012$ , the crumpled composite particles are "open-cell" structure.

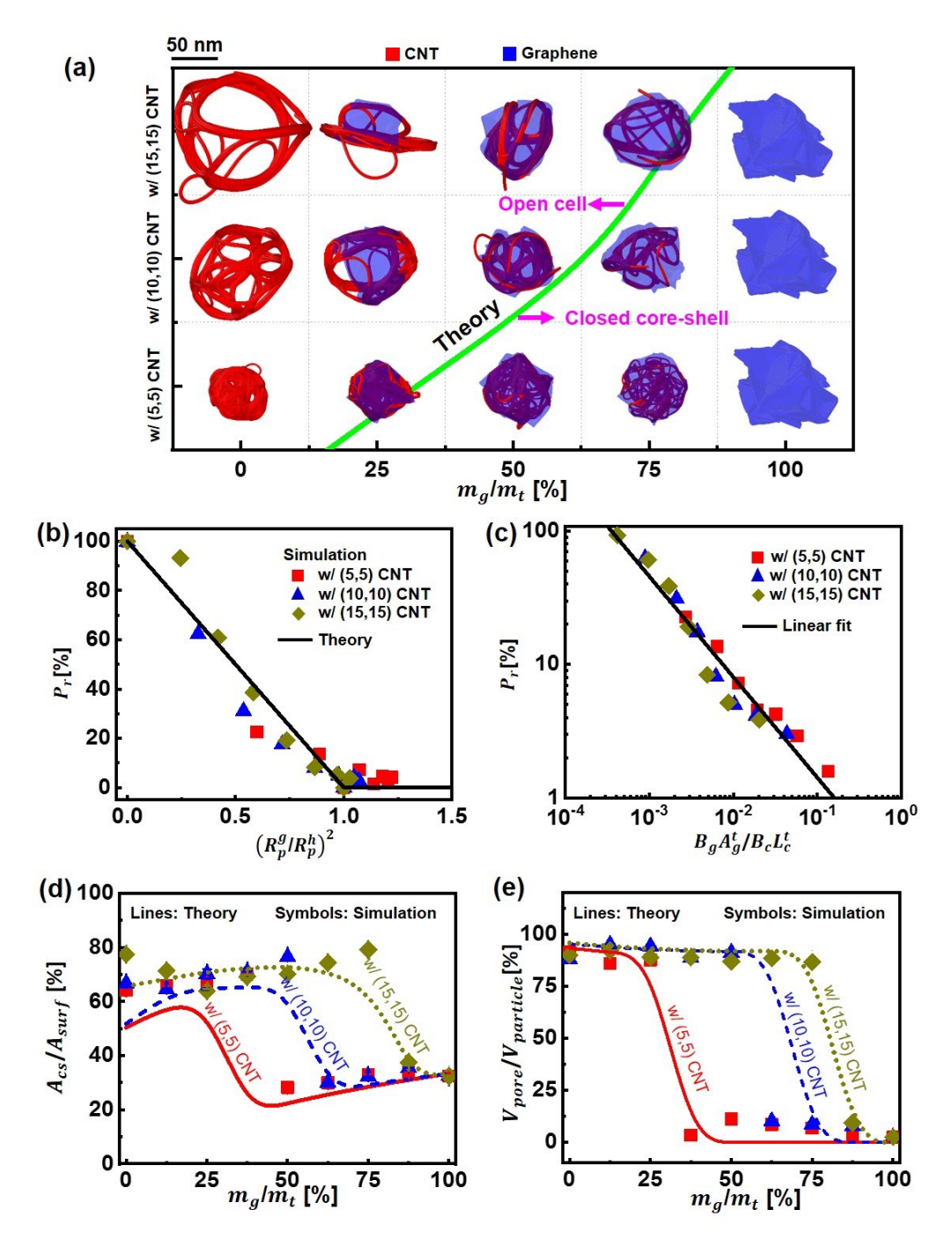


Figure 3. Characterization of interconnected spatial networking structures in the crumpled graphene/CNTs composite particles. (a) Simulation snapshots on spatial networking structures, size and morphology of the crumpled particles obtained at different  $m_g/m_t$  and sizes of CNTs. (b) Comparison of theoretical predictions and simulations on the surface pore ratio  $(P_r)$  of the crumpled particles with the crumpling intensity  $R_p^g/R_p^h$ . (c) Variation of  $P_r$  with the unified intrinsic material parameter  $B_g A_g^t/B_c L_c^t$ . (d) Specific accessible surface area of particles  $(A_{cs})$  normalized by the intrinsic specific area of CNTs and graphene  $(A_{surf})$  versus  $m_g/m_t$  with different sizes of CNTs. (e) Normalized spatial pore volume of particles  $(V_{pore})$  by the overall volume of composite particles  $(V_{particle})$  versus  $m_g/m_t$  with different sizes of CNTs.

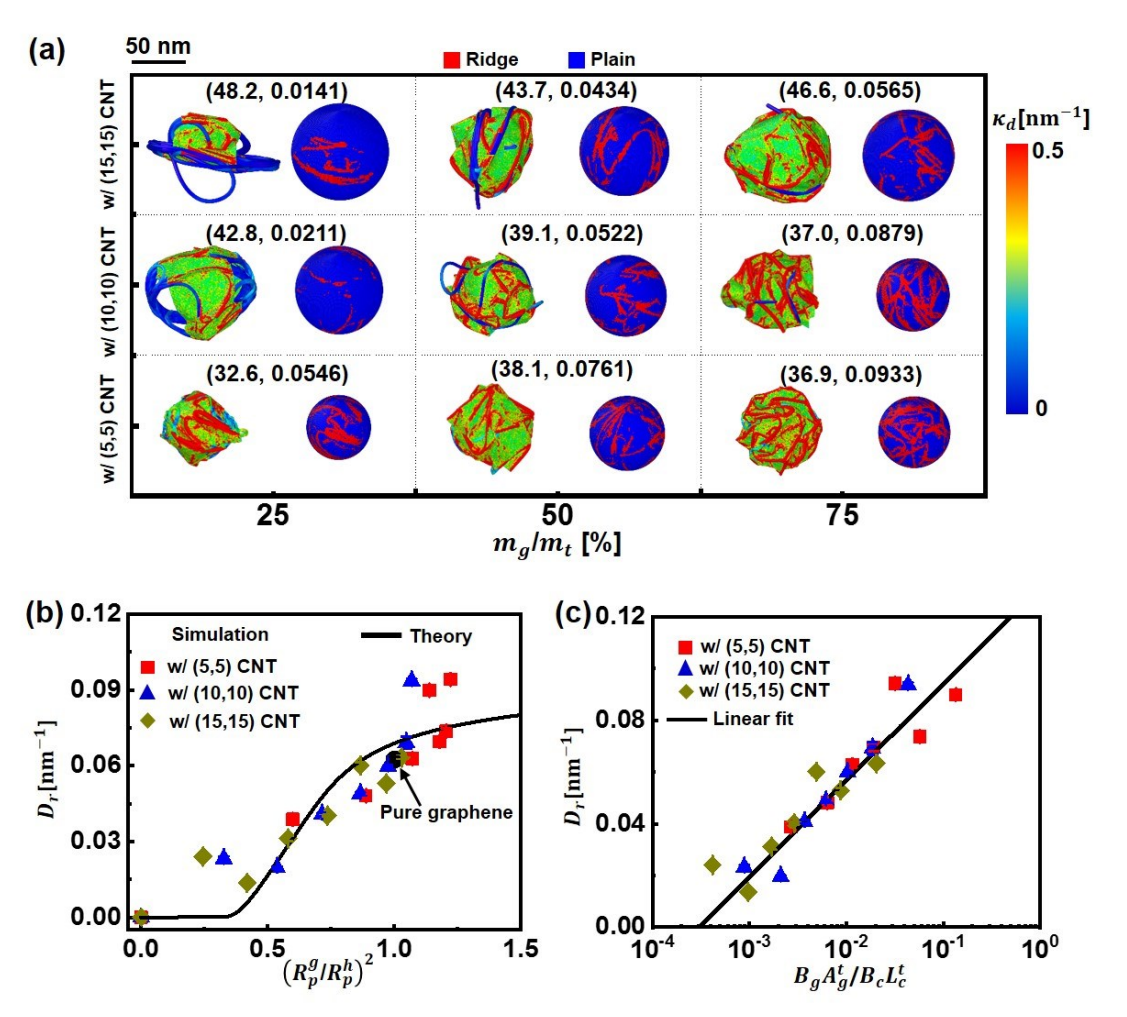


Figure 4. Surface crumpling morphology and local ridge distribution in the crumpled graphene/CNTs composite particles. (a) Simulation snapshots showing the local surface curvature distribution in the particles (left) and their equivalent spheres highlighting the size and ridge distribution (right). The inset bracket "()" in each block represents the radius  $(R_p^h)$ , in nm), and ridge density  $(D_r)$ , in nm<sup>-1</sup> of the crumpled particle. (b) Comparison of  $D_r$  between the theoretical predictions and simulation results with the crumpling intensity  $((R_p^g/R_p^h)^2)$ . (c)  $D_r$  as a function of unified intrinsic material parameter  $B_g A_g^t/B_c L_c^t$ .

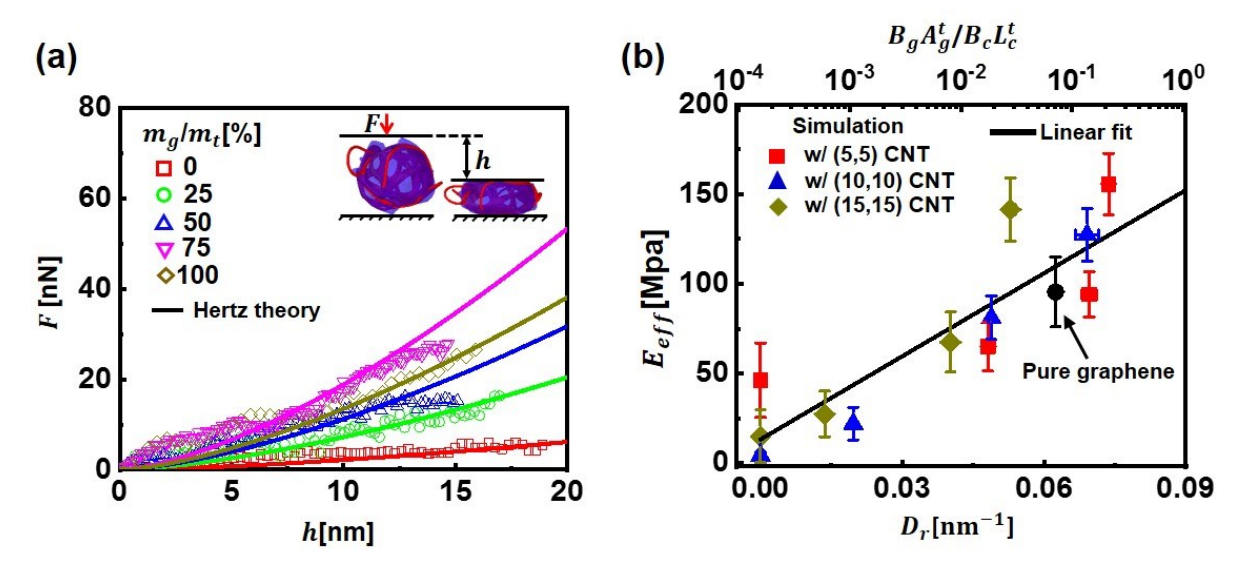


Figure 5. Mechanical performance of individual crumpled graphene/CNTs composite particles. (a) Force-displacement curves of the crumpled graphene/(10,10)CNT particles with different  $m_g/m_t$  along the uniaxial compression z-direction. The insets illustrate the schematics of molecular dynamics simulation model of uniaxial compression experiments on a single particle. (b) Correlation of elastic modulus  $(E_{eff})$  with the ridge density  $(D_r)$  of the crumpled particles and the unified material parameter  $B_g A_g^t/B_c L_c^t$ .  $E_{eff}$  is the averaged Young's modulus by performing uniaxial compression experiments along x, y, and z-directions.

# TOC

